Comparison of different models of cyclone prediction performance for various operating conditions using a general software

S. Altmeyer*, V. Mathieu, S. Jullemier, P. Contal, N. Midoux, S. Rode, J.-P. Leclerc

Laboratoire des Sciences du Génie Chimique de Nancy, CNRS-ENSIC, 1, rue Grandville, BP 451, 54001 Nancy Cedex, France

Abstract

A new software is presented which allows to calculate cyclone efficiency for a given geometry or to determine a geometry for a desired efficiency is presented. It has been established for cyclones with relatively low solids loading (<10 g/m^3) and it applies for pressure drop between 10 and 10 000 Pa, for cut diameter between 0.2 and 20 μm, for volumetric flow rate from 10^{-4} to 1000 m^3/s and for cyclone diameter from 0.01 to 3 m. The calculations are realised with four models presented in the literature. Comparison between model predictions and published measurements, shows that models used in the software predict pretty well the experimental results, obtained in a large range of operating conditions. Moreover, a comparison of the results obtained with these four models permits to select the model the most adapted, depending on inlet flow rate, temperature and pressure used.
© 2003 Elsevier B.V. All rights reserved.

Keywords: Cyclone prediction; Cyclone efficiency; General software; Gas-solid separators; Cyclone design

1. Introduction

Cyclones are mostly used for removing industrial dust from air or process gases. They are the most frequently encountered type of gas–solid separator in industry. The primary advantages of cyclones are economy, simplicity in construction and ability to operate at high temperatures and pressures.

The principle of cyclone separation is simple: the gas–solid mixture enters on the top section. Then, the cylindrical body induces a spinning, vertical flow pattern to the gas–dust mixture. Centrifugal force separates the dust from gas stream: the dust travels to the walls of the cylinder and down the conical section to the dust outlet and the gas exits through the vortex finder.

The choice of cyclone geometry is difficult and often empirical. In order to assist this choice, a software CYCLONE was created which permits to calculate efficiency of cyclone for a known geometry or to determine a geometry for a desired efficiency.

Four models were chosen to realise the calculations. The results of the four calculation models are compared with experimental data found in the literature for different inlet flow rates, pressures and temperatures. In the literature, there are only a few reports comparing different models [1,2], the software presented here allows to compare easily the different models and to propose the most adapted one for different possible operating conditions.

Numerical calculations are more and more used to simulate the flow field in a cyclone [3,4]. However, up to now computational fluid dynamics (CFD) simulations do not allow to evaluate correctly the efficiency. Semi-empiric models remains are, therefore, still very useful to design cyclones.

2. Design of a cyclone

2.1. Selected cyclone design

Cyclone exists under different forms but the reverse flow cyclone represented in Fig. 1 is the most common design used industrially. The cyclone consists of four main parts: the inlet, the separation chamber, the dust chamber and the vortex finder.

Two types of inlet are available: the axial and the tangential inlets shown in Fig. 2. When using an axial inlet, the ro-

---

* Corresponding author.
E-mail address: progepi@ensic.inpl-nancy.fr (S. Altmeyer).
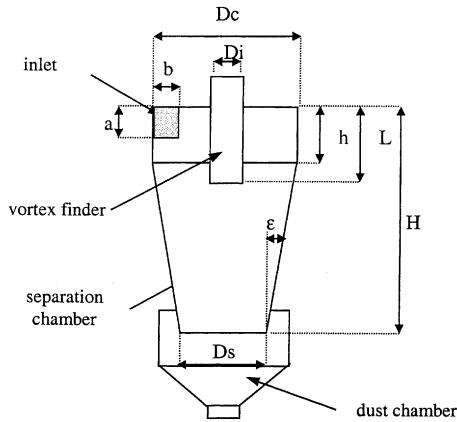
Fig. 1. Cyclone design configuration.
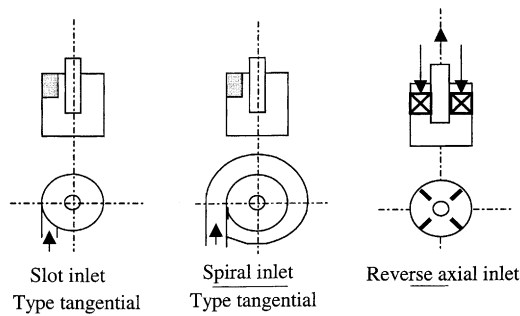
Fig. 2. Type of inlet constructions.

tating flow is generated by guide blades, which distribute the gas flow over the whole circumference of the cyclone. This construction is widely used for the separation of droplets from gases. Tangential inlets are preferred for the separation of solid particles from gases. For the moment, the software deals with the most standard case of reverse flow cyclone with a tangential rectangular inlet.

2.2. Description of the chosen models

Since the first application of aerocyclones in 1886, several models have been developed for the calculation of the design parameters, pressure drop and efficiency. All these approaches can be divided into six groups:

- Mathematical and numerical models.
- Diffusion models.
- Characteristic number models.
- Residence time models.
- Force balance models.
- Models, which combine aspects of the force balance and the résidence time model.

Bohnet et al. [1] realised an analysis which showed that force balance models and combined models are best suited for the calculation of aerocyclone. Due to the physically simplified assumptions (characteristic number and residence time) and the high calculation expenditure (numerical and

diffusion models), the use of the first four models is rather limited.

We have thus chosen four models based on the best suited models:

- Barth [1].
- Leith and Licht [2,5,6].
- Mothes and Löffler [7].
- Lorenz [8].

The first two models are based on force balance and the following two on a combination of force balance and residence analysis. The following part presents some of the elements used to conceive these models. The aim is to present the assumptions made and the principle of calculation of the models.

2.2.1. First considerations

Some assumptions are common to all these models and can be consider reasonable enough to obtain a good compromise between accurate prediction and simplification of the equations. They are:

- The particles are spherical.
- The particle motion is not influenced by the presence of neighbouring particles.
- The radial velocity of the gas equals zero.
- The radial force on the particle is given by Stokes's law.

2.2.2. Barth model

Barth (cited in [1]) proposed a simple model based on a force balance. This model enables to obtain the cut-size and the pressure drop values. The principle of calculation consists on the fact that a particle carried by the vortex endures the influence of two forces: a centrifugal force Z and a flow resistance W. They are expressed at the outlet radius R_i where the highest tangential velocity occurs:

$$W = c_w \frac{\pi}{4} d_{pc}^2 \frac{\rho}{2} w_r^2 \qquad (1)$$

$$Z = \frac{\pi}{6} d_{pc}^3 (\rho_p - \rho) \frac{u^2}{r} \qquad (2)$$

$$C_w = \frac{24}{Re_p} = \frac{24\mu}{d_{pc} w_r(R_i)\rho} \qquad (3)$$

The tangential velocity at R_i equals:

$$w_r(R_i) = \frac{V_0}{2\pi R_i (H - L)} \qquad (4)$$

The radial velocity $u(R_i)$ equals:

$$u(R_i) = \frac{\frac{V_0}{\pi R_i^2}}{\frac{S_e}{S} \frac{\alpha}{\frac{R\alpha}{R_i}} + \lambda \frac{h_{eq}}{R_i}} \qquad (5)$$

where:

$$h_{eq} = \frac{S_{tot}}{2\pi \sqrt{\frac{R_c}{R_i}}} \qquad (5.1)$$

Table 1
Geometry used to test the model of Barth

D_c (m)	D_i/D_c	a/D_c	b/D_c	h/D_c	L/D_c	H/D_c	D_s/D_c
0.15	0.33	0.53	0.13	0.69	0.73	2.58	0.33

$$\alpha = 1 - \left(0.54 - \frac{0.153}{\frac{S_e}{S}}\right)\left(\frac{b}{R_c}\right)^{1/3} \tag{5.2}$$

$$\lambda = 0.05 + \frac{287.4}{Re_w} \tag{5.3}$$

$$Re_w = \frac{D_c \cdot \rho}{\mu} \cdot \frac{V_0}{ab\left(0.089 - 0.204\dfrac{b}{R_c}\right)} \tag{5.4}$$

α is a correction factor for contraction, expressed as a function of the inlet geometry (the equation presented shows the case of a rectangular tangential inlet) and λ a friction factor either equals to 0.02 or a function of the inlet geometry and the inlet flow rate described by Muschelknautz and Brunner [18].

The pressure drop is resolved into two terms. The first term ζ_i reflects the contribution by inlet losses and friction losses. The second term ζ_e results from the flow losses through the outlet pipe.

$$\Delta P = (\zeta_e + \zeta_i)\frac{\rho}{2}w^2(R_i) \tag{6}$$

with:

$$\zeta_e = \frac{R_i}{R_c}\left(\frac{1}{\left(1 - \frac{u(R_i)h_{eq}}{w(R_i)R_i}\lambda\right)^2} - 1\right)\left(\frac{u(R_i)}{w(R_i)}\right)^2 \tag{6.1}$$

$$\zeta_i = f\left(2 + 3\left(\frac{u(R_i)}{w(R_i)}\right)^{4/3} + \left(\frac{u(R_i)}{w(R_i)}\right)^2\right) \tag{6.2}$$

This model is relatively simple but it allows to obtain easily an approximation of the pressure drop and the cut diameter which are the two main parameters for an industrial approach.

The validity of this model was confirmed by comparing its predictions with experimental values obtained under the experimental conditions presented in Tables 1 and 2 [1].

2.2.3. Leith and Licht model

This model [2,5,6] takes into account the temperature and provides the cut-diameter, the pressure drop and the efficiency of separation for a particle of diameter d_p.

Table 2
Experimental conditions used to test the model of Barth (charge load not specified)

V_{inf} (m^3/s)	V_{sup} (m^3/s)	T (K)	P
0	0.033	293	Atm

Leith and Licht describe particle motion in the entry and collection regions with the additional following assumptions:

- The tangential velocity of a particle is equal to the tangential velocity of the gas flow, that is, there is no slip in the tangential direction between the particle and the gas.
- The tangential velocity is related to the radius by: uR^n=constant.

A force balance and an equation on the particles collection yields Eq. (7):

$$\eta = 1 - \exp\left[-2\left(\frac{G\tau V_0}{D_c^3}(n+1)\right)^{0.5/n+1}\right] \tag{7}$$

where:

$$G = \frac{4D_c(2V_s + V)}{a^2 b^2} \tag{7.1}$$

$$n = 1 - \left(1 - \frac{(12D_c)^{0.14}}{2.5}\right)\left(\frac{T + 460}{530}\right)^{0.3} \tag{7.2}$$

$$\tau = \frac{\rho_p d_p^2}{18\mu} \tag{7.3}$$

Note: G is a factor related to the configuration of the cyclone, n is related to the vortex and τ is the relaxation term.

The pressure drop is described by Eq. (8):

$$\Delta P = 0.003\rho\left(\frac{16V_0^2}{abD_i^2}\right) \tag{8}$$

The cut-size is given by Eq. (9):

$$d_{pc} = \sqrt{\frac{9\mu D_c ab}{4\pi N_t V_0(\rho_p - \rho)}} \tag{9}$$

where

$$N_t = \frac{V_0}{ab}$$
$$\times\left(0.1079 - 0.00077\frac{V_0}{ab} + 1.924\times 10^{-6}\times\left(\frac{V_0}{ab}\right)^2\right) \tag{9.1}$$

N_t is the number of times the gas turned around in the cyclone between its inlet and its outlet and is a function of the flow rate and the inlet geometry.

This model is easy to handle. Moreover, it takes temperature into account via its influence on efficiency but it is based on simplified physicals assumption. Lorenz [8] shows that the efficiency for the small particles calculated with this model is higher than that calculated with the others models.

The validity of this model was confirmed by comparing its predictions with experimental values obtained under the experimental conditions presented in Tables 3 and 4 [2,6].

Table 3
Geometry used to test the model of Leith and Licht

	D_c (m)	D_i/D_c	a/D_c	b/D_c	h/D_c	L/D_c	H/D_c	D_s/D_c
Geometry 1	0.2032	0.5	0.5	0.2	1.5	0.5	4	0.375
Geometry 2	0.3048	0.5	0.583	0.208	1.33	0.583	3.166	0.5
Geometry 3	0.2794	0.527	0.841	0.264	1.527	1.055	2.873	0.527
Geometry 4	0.4699	0.527	0.838	0.254	1.524	1.054	2.865	0.527

Table 4
Experimental conditions used to test the model of Leith and Licht (charge load not specified)

V_{inf} (m³/s)	V_{sup} (m³/s)	T_{inf} (K)	T_{sup} (K)	P
0.06	0.13	310	422	atm

2.2.4. Lorenz model

This model [8] based on the four assumptions below, takes into account the temperature and provides the cut-diameter, the pressure drop and the efficiency of separation for a particle of diameter d_p.

2.2.4.1. Hypotheses.

- The tangential velocity depends only on the coordinate R and not on the axial coordinate (z).
- The particle motion is determined as the sum of a random movement (due to the gas) and a collective movement (due to the flow of particles).
- For the removal of particles from the gas, the particles must be prevented from entering the upward flow into the exit and must deposit on the wall of the cyclone during their residence time.
- Re-entrainment of already deposited particles from the conic part is essentially due to the increasing turbulent back-mixing of particles on the cyclone bottom.

The model is based on calculations made on the cyclone subdivided into five parts as presented in Fig. 3.

The principle of the model is to form a differential system with mass balances in each region. The equations of the system depend on the geometry, the inlet flow rate and the two following main parameters:

- $j_i(z)$: particle flux at the height z and in the region i.
- $c_i(z)$: concentration of particles at the height z and in the region i.

2.2.4.2. Parameters used in the system.

Equivalent cyclone. For the commodity of the calculation, Lorenz defines an equivalent cyclone of same height H and of radius R_c^*.

$$R_c^* = \sqrt{\frac{V_{cyclone}}{\pi H}} \tag{10}$$
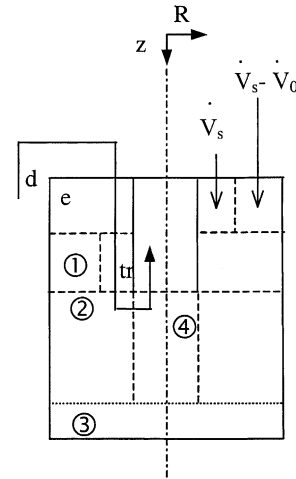
Region d, e, tr : Regions of the boundary layer flow
Region 1   :   Entrance region
Region 2   :   Region of downstream flow
Region 3   :   Region of re-entrainment
Region 4   :   Region of upstream flow

Fig. 3. Cyclone geometry used in calculations of Lorenz.

The secondary flow. The secondary flow is in the boundary layer along the cover plate and the outside of the vortex. This flow has to be considered because the boundary layer carries particles, which can reach the cyclone outlet without entering into the separation zone. Lorenz calculates it using equations from Ebert (cited in [8]) where n is the vortex exponent, δ_d the absolute boundary layer thickness and Φ is a shape factor for the flow profile of the boundary layer.

$$V_s = 2\pi R_c u(R_c) \left(\frac{R_i^*}{R_c}\right)^{1-n} \delta(R_i^*)(0.26 - 0.154\Phi) \tag{11}$$

with:

$$\delta_d = f(R/R_c,\ Re) \tag{11.1}$$

$$n = \frac{\ln(u(R)/u(R_c))}{\ln(R_c/R_i)} \tag{11.2}$$

$$\Phi = -0.1 \tag{11.3}$$

$$R_i^* = R_i + 0.053R_c \tag{11.4}$$

R_i^* is the equivalent radius of the engagement length of cyclone. It is the sum of the real radius R_i and the thickness of the boundary layer of the tube.

The tangential velocity. The tangential velocity at R is calculated using the equations derived by Meissner (cited in [10])

$$u(R) = \frac{u(R_c)}{\frac{R}{R_c}\left(1 + \vartheta\left(1 - \frac{R}{R_c}\right)\right)} \tag{12}$$

with

$$\vartheta = \frac{u(R_c)}{w(R_c)}\left(\lambda_{cyl} + \frac{\lambda_{cone}}{\sin \varepsilon}\right)$$

In this equation θ is the angular momentum that characterises the angular momentum exchange between the wall and the gas. θ is a function of the velocities $u(R_c)$, $w(R_c)$ and of λ_i: friction coefficients (λ_{cyl}, λ_{cone}). All the values λ_i are considered constant. Usually this coefficient was considered equal to 0.007. Lorenz improved the previous models by using the following formula:

$$\lambda = \lambda_0(1 + 2\sqrt{\varphi_e}) \tag{12a}$$

where:

$$\lambda_0 = 0.005 + \frac{287.4}{Re_w} \tag{12.1}$$

$$Re_w = \frac{u'(R_c)D_c\rho}{\mu} \tag{12.2}$$

$$u'(R_c) = \frac{V_0}{ab\left(0.889 - 0.204\frac{b}{R_c}\right)} \tag{12.3}$$

φ_e : inlet charge (kg/kg)

Diffusivity due to turbulence. In the case of radial exchange of particles, the model needs to take into account the diffusivity by the coefficient: D_{turb} given by Eq. (13):

$$D_{turb} = 0.006\left(1 + \arctan\left[\frac{Re_{tr}}{136\,864}\right]\right) \tag{13}$$

Settling velocity.

$$w_s(R) = \frac{(\rho_p - \rho)d_p^2 u^2(R)}{18\mu R} \tag{14}$$

Radial velocities.

$$w(R_c) = 0 \tag{15}$$

$$w(R_i) = \frac{(V - V_s)}{2\pi R_i(H - L)} \tag{16}$$

Re-entrainment of particles. The re-entrainment of particles already separated in the lower part is taken into account. The highest possible re-entrained mass flow is defined by the equation below:

$$m_w = m_{w,max} \cdot w(Re_s) \tag{17}$$

with:

$$m_{w,max} = V_0 c_0 - V(L)c_4(L) - V_s c_{tr}(L) \tag{17.1}$$

$$w(Re_s) = 0.375 - 0.238 \arctan\left(\frac{Re_s - 35\,776}{10\,548}\right) \tag{17.2}$$

Flow rate at z.

$$\begin{cases} V(z) = 0 & \text{for}: \ 0 \le z \le L \\ V(z) = (V_0 - V_s)\dfrac{(H - z)}{(H - L)} & \text{for}: \ L \le z \le H \end{cases} \tag{18}$$

2.2.4.3. Equations of the differential system. The system of differential equations is obtained by writing mass balances in each region, by calculating the particle concentration on the axial co-ordinate z. The system is solved using boundary conditions.

2.2.4.4. Determination of the parameters.

2.2.4.4.1. Efficiency.

$$\eta = 1 - \frac{\dfrac{V_s}{V_0}c_{tr}(L) + \dfrac{V_0 - V_s}{V_0}c_4(L)}{c_0} \tag{19}$$

2.2.4.4.2. Pressure drop.

$$\Delta P = \xi \frac{\rho}{2}w^2(R_c) \tag{20}$$

with:

$$\xi = \xi_e + \xi_{stat} + \xi_{dyn} + \xi_i \tag{20.1}$$

$$\xi_e = \left(\frac{u'(R_c)}{w(R_c)}\right)^2 - \left(\frac{u(R_c)}{w(R_c)}\right)^2 \tag{20.2}$$

$$\begin{aligned}\xi_{stat} = &\left(\frac{u(R_c)}{w(R_c)}\right)^2\frac{2}{(1+\vartheta)^4}\\ &\times\left[\frac{1}{2R^4U^2} + \frac{3\vartheta}{R^2U} - 3\vartheta\ln(R^2U) - \vartheta^3 R^2 U - 3\vartheta \right. \\ &\left. -0.5 + \vartheta^3\right]\end{aligned} \tag{20.3}$$

$$\xi_{dyn} = \left(\frac{u(R_c)}{w(R_c)}\right)^2(1 - U^2) \tag{20.4}$$

$$\xi_i = 0.74\left[2 + 3\left(\frac{u(R_i)}{w(R_i)}\right)^{4/3} + \left(\frac{u(R_i)}{w(R_i)}\right)^2\right]\left(\frac{R_c}{R_i}\right)^4 \tag{20.5}$$

U and R are dimensionless terms:

$$U = \frac{u(R_i)}{u(R_c)}, \quad R = \frac{R_i}{R_c} \tag{21}$$

This model yields a complex calculation procedure. It takes the temperature, via its influence on the diffusion coefficient and on the friction factor, the re-entrainment and the

Table 5
Geometry used to test the model of Lorenz

	D_c (mm)	D_i/D_c	a/D_c	b/D_c	D_s/D_c	H/D_c	h/D_c	L/D_c
Geometry 1	150	0.33	0.53	0.13	0.33	2.58	0.69	0.73
Geometry 2	150	0.23	0.53	0.13	0.33	2.58	0.69	0.73
Geometry 3	150	0.23	0.40	0.10	0.33	2.58	0.69	0.73

Table 6
Experimental conditions used to test the model of Lorenz (charge load not specified)

V_{inf} (m³/s)	V_{sup} (m³/s)	T_{inf} (K)	T_{sup} (K)	P
0	0.056	293	1123	atm

Table 8
Experimental conditions used to test the model of Mothes and Löffler (charge load not specified)

V_{inf} (m³/s)	V_{sup} (m³/s)	T_{inf} (K)	T_{sup} (K)	P
0.06	0.13	310	422	atm

secondary flux into account. The results obtained are satisfactory. However, in the work of Lorenz, this model is established and tested with three geometries only (cf. Table 5) and the parameter are fitted to the experimental results. Not surprisingly, the model is very adequate for these three geometries but it must be verified for the others.

The prediction of this model were compared with results obtained at the experimental conditions presented in Tables 5 and 6 [1,8].

2.2.5. Mothes and Löffler model

As the model of Lorenz, this model yields the cut-diameter, the pressure drop and the efficiency of separation for a particle of diameter dp. Mothes and Löffler [7] established a model on the principle described previously in the model of Lorenz. They were the first to propose a model based on a differential system of equations by separating the cyclone into four parts. The following assumptions were made which simplify the system:

- λ and D_{turb} are supposed constant
  - $\lambda = 0.007$
  - $D_{turb} = 0.0125$
- There is no re-entrainment
  - $m_w = 0$
- Mothes and Löffler consider that there is no separation in the region 1 above $a/2$, which implies that there is no regions d, e and tr.
  - No secondary flow ($V_s = 0$).

At room temperature, the results obtained with this model are satisfactory. But it becomes less satisfactory at high temperature [8]. For example the error corresponding to the pressure drop could reach more than 50% at temperature between 700 and 850 °C.

The reasons, which can explain the difference between the experimental, and the theoretical results are the following:

- The friction coefficient λ is taken constant, therefore, it is implicitly assumed that the viscosity has no influence on the friction.
- Re-entrainment of particles is not taken into account in the calculation
- The coefficient of diffusivity is taken constant. Therefore, it is not dependent on the flow.
- The coefficient of pressure drop is only dependent on the geometry and not on the volumetric flow rate, the viscosity or the density.

This model was compared with data obtained at the experimental conditions presented in Tables 7 and 8 [7].

2.3. Software used for the calculation

The software CYCLONE (cf. Fig. 4) enables to calculate efficiency of a cyclone for a known geometry or to give a geometry for a desired efficiency.

The four models described previously are available in the software. The knowledge of some parameters is necessary to make the calculation:

- gas characteristics (temperature, pressure, viscosity and density)
- solid characteristics (solid distribution and density)

The software gives the choice between defined configurations of the cyclone used by the conceivers of models. These classical geometries are reported in the Table 9. The interesting point is that, once the configuration is chosen, there is just one parameter (cyclone diameter) to evaluate to obtain all cyclone dimensions. It is also possible to use its own geometry.

Table 7
Geometry used to test the model of Mothes and Löffler

	D_c (m)	D_i/D_c	a/D_c	b/D_c	h/D_c	L/D_c	H/D_c	D_s/D_c
Superior values	0.095	0.779	1.05	0.316	7.579	7.579	0.307	0.779
Inferior values		0.421		0.158	2.41	2.41	3.231	0.421
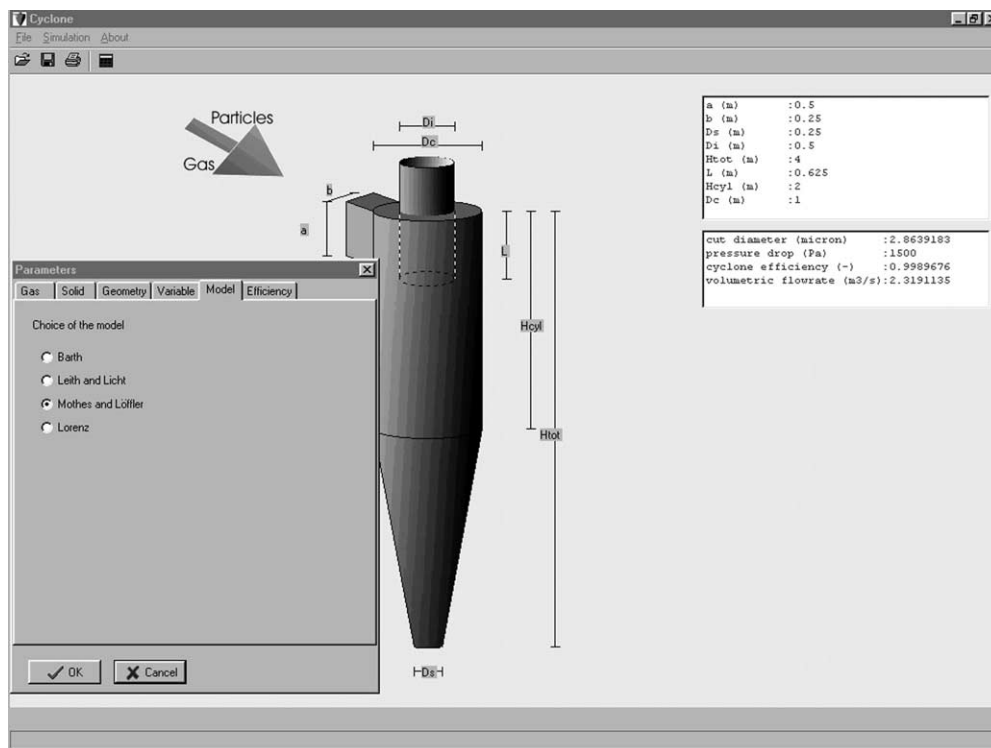
Fig. 4. Graphic interface of the software 'CYCLONE'.

Table 9
Geometric ratios for eight models

	a/D_c	b/D_c	D_s/D_c	D_i/D_c	H/D_c	L/D_c	h/D_c
LAPPLE	0.5	0.25	0.25	0.5	4	0.625	2
SWIFT1	0.5	0.25	0.4	0.5	3.75	0.6	1.75
SWIFT2	0.44	0.21	0.4	0.4	3.9	0.5	1.4
STAIRMAND	0.5	0.2	0.375	0.5	4	0.5	1.5
PETERSON and WHITBY	0.583	0.208	0.5	0.5	3.173	0.583	1.333
LORENZ1	0.533	0.133	0.333	0.333	2.58	0.733	0.693
LORENZ2	0.533	0.133	0.333	0.233	2.58	0.733	0.693
LORENZ3	0.4	0.1	0.333	0.233	2.58	0.733	0.693

Five parameters are calculated by the software:

- volumetric flow rate,
- cyclone diameter,
- cut diameter,
- cyclone efficiency,
- pressure drop.

To run the software, the user needs to enter two parameters, the other parameters are calculated. The combinations available are:

- volumetric flow rate and cyclone diameter,
- cyclone efficiency and cyclone diameter,
- cut diameter and cyclone diameter,
- pressure drop and cyclone diameter,
- cyclone efficiency and volumetric flow rate,
- cut diameter and volumetric flow rate,
- pressure drop and volumetric flow rate.

For the following combinations, the user needs to indicate in addition the order of magnitude of the volumetric flow rate.

- pressure drop and cyclone efficiency,
- pressure drop and cut diameter.

The following part compares the results obtained by the four models depending on inlet flow rate, temperature and pressure used.

3. Choice of the most adequate model

This part allows to choose the most adequate model depending on inlet flow rate, temperature and pressure used.

In order to realise this part, the results calculated with the software with the four models were compared with experimental data found in the literature [9–18]. The range

Table 10
Limiting values of the experimental conditions

	Minimal value	Maximal value
P (bar)	1	15.6
T (K)	293	1300
Density (kg/m^3)	860	3900
D_c (m)	0.023	0.4
Volumetric flow rate (m^3/s)	0.00005	0.25
Charge load (g/m^3)	0.8	10

Table 11
Other geometries

Other geometry	a/D_c	b/D_c	D_s/D_c	D_i/D_c	H/D_c	L/D_c	h/D_c
Geometry 1	0.5	0.25	0.25	0.5	3.98	1.06	1.99
Geometry 2	0.38	0.19	0.38	0.31	4.31	1.13	1.81

of the experimental conditions used in these references is summarised in Table 10. The other geometries used in the software are summarised in Table 11.

3.1. Definition of the cut size

3.1.1. Evolution of the cut-size with inlet flow rate

The flow rate influences strongly the results as indicated by several reports: Mothes and Löffler [12], Ray et al. [11], Patterson and Munz [9] and Xiang et al. [15]. The tangential velocity increases with an increase of the inlet velocity, leading to a greater degree of separation in centrifugal separators. Therefore, the cut-size decreases with increasing flow rate.

Fig. 5 shows an example of cut-size variation with inlet velocity according to Patterson and Munz [9]. It appears that for inlet velocity higher than 5 m/s, the models of Lorenz and Mothes and Löffler predict quite well experiments' results.
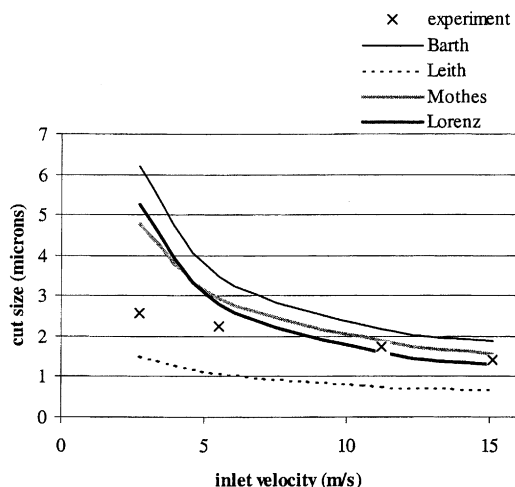
Fig. 5. Evolution of cut-size with inlet velocity. Comparison between experiments made by Patterson and the results obtained with the four models ($P = 1$ bar, $T = 293$ K, $d = 3900$ kg/m^3, $D_c = 0.102$ m, geometry 1 (Table 11)).
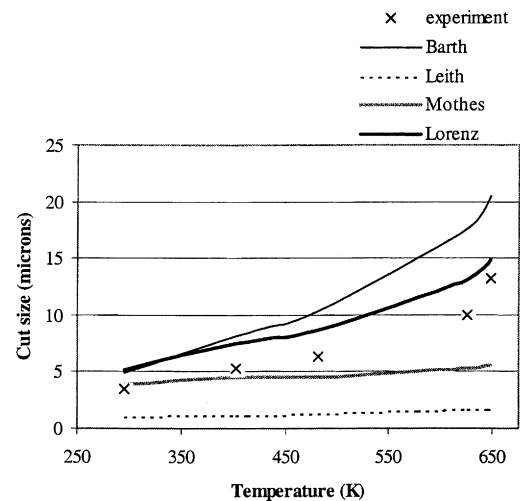
Fig. 6. Cut-size as a function of temperature. Comparison between experiments made by Parker et al. [10] and the results obtained with the four models ($P = 1.9$ bar, $d = 2300$ kg/m^3, $u_i = 1.77$–2 m/s, $D_c = 0.058$ m, geometry 2 (Table 11)).

This result is confirmed by the comparison made with data of the other authors. However, at an inlet velocity below 5 m/s, Fig. 5 shows that the model of Leith and Licht gives better predictions. The other authors do not work at such low inlet velocities.

3.1.2. Evolution of the cut-size with the temperature

Cyclones are often used industrially at high temperature, but unfortunately, the experimental studies realised in laboratories are made at room temperature and there is a lack of data concerning experiments at high temperature. However, the work of Patterson and Munz [9], and Parker et al. [10] present high interest.

The cut-size increases significantly with temperature. According to Fig. 6, the model of Mothes and Löffler gives a good estimate of the cut-size for temperature below 450 K. At temperature higher than 450 K, the model of Lorenz gives better predictions.

3.2. Study of pressure drop

3.2.1. Evolution of pressure drop with inlet flow rate

The articles of Patterson and Munz [9] and of Mothes and Löffler [12] were used. It appears that accuracy of results is highly dependent on values of inlet flow rate. Pressure drop increases with flow rate. Even if a higher flow rate tends to improve the separation, it is not relevant to work at very high flow rate, because of the important increase of pressure drop. In the case of a small inlet flow rate, the model of Barth [1] gives the best result. However, at higher flow rate, the model of Lorenz and Mothes [12] yields better results.

Fig. 7 shows an example of pressure drop variation with inlet flow rate (Patterson and Munz).
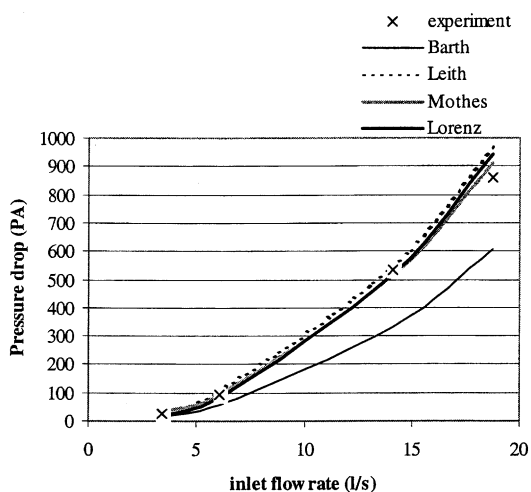
Fig. 7. Evolution of pressure drop with inlet flow rate. Comparison between data presented by Patterson and Munz and the predictions of the four models ($P = 1$ bar, $T = 293$ K, $d = 3900$ kg/m^3, $D_c = 0.102$ m, geometry 1 (Table 11)).

3.2.2. Evolution of pressure drop with temperature

The pressure drop decreases significantly with rising temperature. This effect is mainly due to the decrease of the density and the increase of the viscosity of the gas.

According to Fig. 8, the models of Barth and of Lorenz give quite a good approximation of the pressure drop. However, Barth's model does not take into account temperature in its calculations: its predictions are, therefore, not reliable. Using the data of Patterson and Munz, the four models are equivalent, with an error in the prediction of about 80%.

3.3. Study of separation efficiency

3.3.1. Evolution of separation efficiency at room conditions

Separation efficiency at room temperature was studied using experimental data of Yoshida et al. [13], Xiang et al.
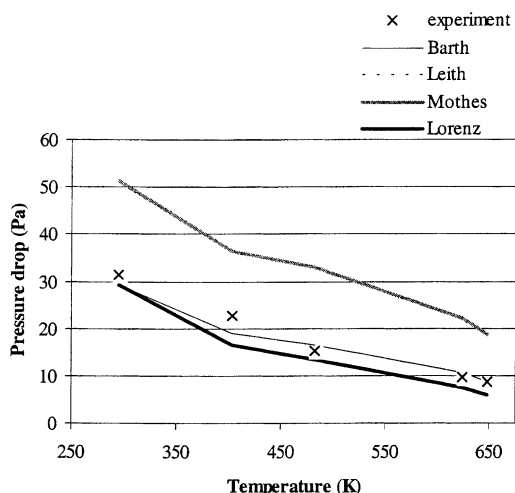
Fig. 8. Pressure drop as a function of temperature. Comparison between data presented by Parker et al. [10] and the predictions of the four models ($P = 1.9$ bar, $d = 2300$ kg/m^3, $u_i = 1.77$–2 m/s, $D_c = 0.058$ m, geometry 2 (Table 11)).
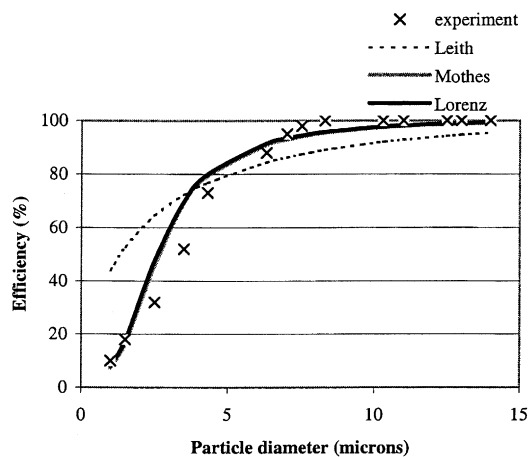
Fig. 9. Separation efficiency results. Comparison between data presented by Ray et al. [11] and the predictions of the three models (Barth's model does not calculate efficiency, $P = 1.7$ bar, $T = 293$ K, $d = 2640$ kg/m^3, $u_i = 11$ m/s, $D_c = 0.4$ m, Stairmand geometry).

[15], Dietz [16] and Ray et al. [11] reports. They all show that the model of Mothes and Löffler and of Lorenz yield excellent predictions at inlet flow rates higher than 10 m/s. An example of this agreement is presented in Fig. 9. However, for smaller flow rates, even if they stay the best models, results are less precise.

3.3.2. Evolution of separation efficiency at high temperature

Parker et al. [10] led experiments at temperature up to 973 K and pressures up to 25 bars. They concluded that the efficiency decreases dramatically as temperature increases from 293 to 993 K.

In order to verify the accuracy of model predictions, the program was run under the same running conditions for the three models. One set of results is presented on Fig. 10. It can
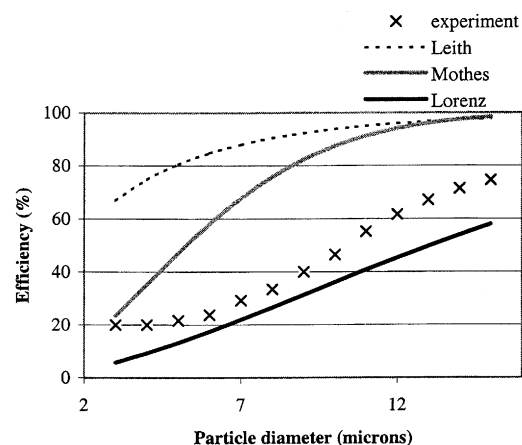
Fig. 10. Separation efficiency. Comparison between data of Parker et al. [10] and the predictions of the three models ($P = 1.9$ bar, $d = 2300$ kg/m^3, $u_i = 1.97$ m/s, $D_c = 0.058$ m, geometry 2 (Table 11)).
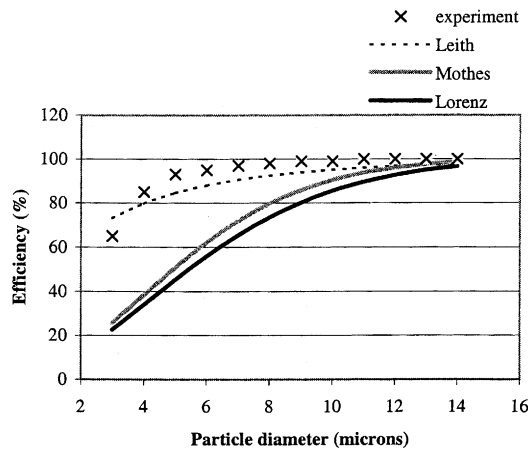
Fig. 11. Evolution of separation efficiency at high pressure. Comparison between data by Parker et al. [10] and the predictions of the three models ($P = 5.16$ bar, $T = 293$K, $d = 2300$ kg/m^3, $u_i = 1.4$ m/s, $D_c = 0.058$ m, geometry 2 (Table 11)).

be seen that only Lorenz model gives a good prediction of experiment values. This is hardly surprising since Lorenz's model is the most developed model of the software in terms of temperature influence.

3.3.3. Evolution of separation efficiency at high pressure

According to the last part, the effect of pressure on efficiency results depends on the temperature chosen for the experiment. Two cases are also distinguished: room temperature and high temperatures.

3.3.3.1. Room temperature.
Parker et al. [10] present data obtained at room temperature and pressure higher than 2 bars. Fig. 11 presents four experiments realised under these conditions. This experiment shows that the model of Leith and Licht yields the better predictions.

3.3.3.2. High temperature.
The data presented by Dietz [16] concern experiments at temperature above 1000 K It appears that the model of Leith and Licht gives here also the best agreement with experiment (Fig. 12a). However, for temperature around 780 K, the model of Lorenz gives the best result (Fig. 12b). According to results of Parker et al. [10] predictions at high temperature are better at high pressure.

3.4. Domain of reliability of the models

Considering the work presented above, conclusions may be drawn that help to choose the best model depending on the operating conditions. Tables 12 and 13, based on all the conclusions extracted from this study, indicate for each experimental condition, the most reliable models.

(a)

(b)
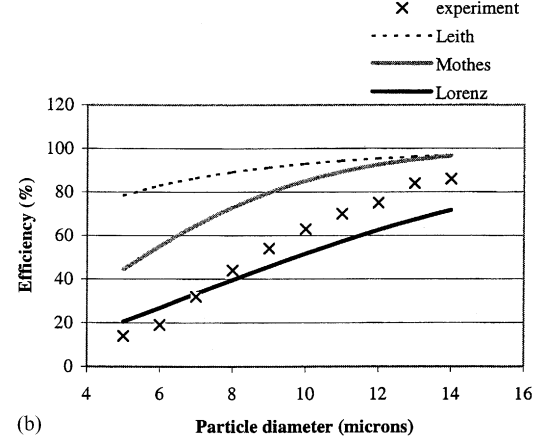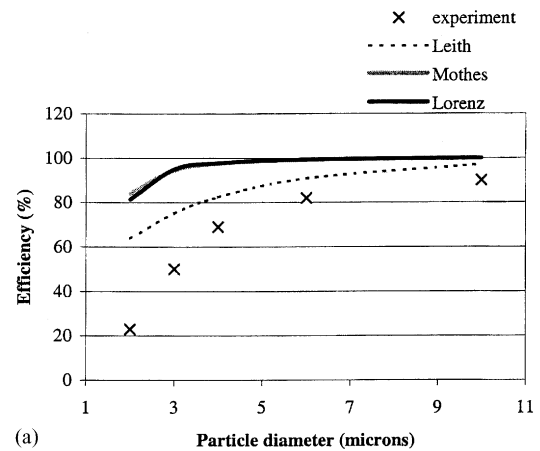
Fig. 12. (a) Evolution of separation efficiency. Comparison between data by Dietz [16] and the predictions of the three models ($P = 6$ bar, $T = 1221$ K, $d = 2500$ kg/m^3, $u_i = 49.4$ m/s, $D_c = 0.2$ m, Swift1 geometry). (b) Evolution of separation efficiency. Comparison between data of Parker et al. [10] and prediction of the three models ($P = 5.16$ bar, $T = 785$ K, $d = 2300$ kg/m^3, $u_i = 1.98$ m/s, $D_c = 0.058$ m, geometry 2 (Table 11)).

Table 12
Comparison of models predictions at different flow rate at room temperature ($T = 293$ K)

	Inlet flow rate, <5 m/s	Inlet flow rate, >5 m/s
Separation efficiency	Lorenz Mothes	Lorenz Mothes Leith and Licht
Cut-size	Leith and Licht	Lorenz Mothes
Pressure drop	Barth	Lorenz Mothes

Table 13
Comparison of models predictions at different pressure and high temperature

	293 < T < 900 K		T > 900 K
	Pressure < 2 bar	Pressure > 2 bar	
Separation efficiency	Lorenz	Lorenz	Leith and Licht
Cut-size	Lorenz Leith and Licht	Lorenz Mothes	Leith and Licht
Pressure drop	Lorenz	Lorenz	Lorenz Mothes Leith and Licht

4. Conclusion

The software CYCLONE presented in this paper offers an easy way to calculate efficiency of a cyclone for a known geometry or to choose geometry for a desired efficiency.

Four calculation procedures for aerocyclone design are used in this software. Studies of literature cases, show that models used in the software predict pretty well the experimental results. Moreover, a comparison of the results obtained with these four models permits to propose the model the most adapted to an operating condition.

Some improvements could be done in the future to make the software more efficient:

- by integrating a solid concentration term: indeed, calculations were made for solid concentration below 10 g/m^3 of gas. If the solid loading exceeds a certain amount, approximately 10 g/m^3, the gas stream is unable to carry all particles. The exceeding solids are moving as a strand directly into the dust chamber. To consider this effect Muschelknautz and Brunner [18] introduced the so-called 'limited solids loading μ_{GR}' which could be integrated in the software.
- By introducing new models: the models of Dietz [16] and Zenz [19], developed in 1981 and 1984, could be added and also the corrections of Clift (see Ghadiri and Hoffman [20]) on the Leith and Licht model in 1991. These three models proved efficient in several works [11,17].

Acknowledgements

Appendix A. Nomenclature

A	width of inlet cross-section (m)
B	height of inlet cross-section (m)
c_i	particle concentration in the region I (kg/m^3)
$C_i(z)$	particle concentration at height z and in the region i (kg/m^3)
c_w	drag coefficient (–)
d_p	particle diameter (m)
d_{pc}	cut-size diameter (m)
D_c	cyclone diameter (m)
D_i	outlet diameter for the gas (m)
D_{turb}	diffusion coefficient (m^2/s)
f	correction factor (depending of the type of pipe)
g	acceleration of gravity (m/s^2)
G	factor describing the geometric configuration (–)
h_{eq}	equivalent height of the cyclone (m)
H	total height of the cyclone (m)
$j_i(z)$	particle flux at the height z and in the region i (kg/m^2 s)
L	engagement length of cyclone (m)

m_w	re-entrained flow (kg/s)
n	vortex coefficient (–)
R	radius (m)
R_c	cyclone radius (m)
R_c^*	radius of the cylindrical part for the equivalent cyclone (m)
R_e	inlet radius of cyclone (m)
R_i	gas outlet pipe radius (m)
R_i^*	equivalent radius of the engagement length of cyclone (m)
R_α	average length from the entry to the centre (m)
Re	Reynolds number (–)
S_e	cross surface area of the cyclone inlet (m^2)
S	cross surface area of the vortex finder inlet (m^2)
S_{tot}	inner area of cyclone (m^2)
T	temperature (K)
u	tangential velocity (m/s)
V	volumetric flowrate at the abscissa z (m^3/s)
V	volume where the vortex turns (m^3)
$V_{cyclone}$	volume of the cyclone (m^3)
V_0	inlet volumetric flow rate (m^3/s)
V_s	secondary volumetric flow rate (m^3/s)
w_s	settling velocity (m/s)
w_r	radial velocity (m/s)
W	flow resistance force (N)
z	axial co-ordonate (–)
Z	centrifugal force (N)

Greek letters

α	correction factor for contraction (–)
δ	thickness of the boundary layer (m)
ε	angle between the conical wall and the vertical (–)
ζ_e	pressure drop from the flow losses through the outlet pipe (Pa)
ζ_i	pressure drop from the inlet losses and friction losses (Pa)
Δp	pressure drop (Pa)
λ	friction factor (–)
η	separation efficiency (–)
ρ	gas density (kg/m^3)
ρ_p	solids density (kg/m^3)
τ	relaxation time (s)
μ	viscosity (Pa s)
θ	angular momentum parameter (–)

References

[1] M. Bohnet, O. Gottschalk, M. Morweiser, Modern design of aerocyclones, Adv. Powder Technol. 8 (2) (1997) 137–161.

[2] D. Leith, W. Licht, The collection efficiency of cyclone type particle collectors—a new theoretical approach, AIChE Symp. Ser. Air Pollut. Control 68 (126) (1996) 196–206.

[3] M.D. Slack, R.O. Prasad, A. Bakker, F. Boysan, Advances in cyclone modelling using unstructured grids, Trans. IChemE 78 (Part A) (2000) 1098–1104.

[4] W.D. Griffiths, F. Boysan, Computational fluid dynamics (CFD) and empirical modeling of a number of cyclone samplers, J. Aerosol Sci. 27 (2) (1996) 281–304.

[5] A.K. Coker, Understand cyclone design, Chem. Eng. Prog. 28 (1993) 51–55.

[6] W. Licht, W.H. Koch, New design approach boosts cyclone efficiency, Chem. Eng. (1977) 80–88.

[7] H. Mothes, F. Löffler, Prediction of particle removal in cyclone separators, Int. Chem. Eng. 28 (2) (1988) 51–55.

[8] T. Lorenz, Heissgasentstaubung mit zyklonen, Vol. 3 (no. 366), VDI-Fortschrittsberichte, Düsseldorf, 1994, pp. 1–113.

[9] P.A. Patterson, R.J. Munz, Cyclone efficiencies at very high temperatures, Can. J. Chem. Eng. 67 (1989) 321–328.

[10] R. Parker, R. Jain, S. Calvert, Particle collection in cyclone at high temperature and high pressure, Environ. Sci. Technol. 15 (4) (1981) 451–458.

[11] M.B. Ray, P.E. Luning, A.C. Hoffman, A. Plomp, M.I.L. Beumer, Post cyclone (PoC): an innovative way to reduce the emission of fines from industrial cyclones, Ind. Chem. Res. 36 (1997) 2766–2774.

[12] H. Mothes, F. Löffler, Motion and deposition of particles in cyclones, Ger. Chem. Eng. 27 (1985) 223–233.

[13] H. Yoshida, A. Sugitate, K. Fukui, E. Shinoda, J. Ma, Effect on the duct shape on particle separation performance of cyclone separator, J. Chem. Eng. Jpn. 33 (2000) 273–276.

[14] L. Enliang, W. Yingmin, A new collection theory of cyclone separators, AIChE J. 35 (1989) 666–669.

[15] R. Xiang, S.H. Park, K.W. Lee, Effects of cone dimension on cyclone performance, Aerosol Sci. 32 (2001) 549–561.

[16] P.W. Dietz, Collection efficiency of cyclone separators, AIChE J. 27 (6) (1981) 888–891.

[17] R.L. Salcedo, Collection efficiencies and particle size distributions from sampling cyclones—comparison of recent theories with experimental data, Can. J. Chem. Eng. 71 (1993) 20–27.

[18] E. Muschelknautz, K. Brunner, Untersuchungen an Zyklonen, Chem. Ing. Technol. 39 (1967) 531–538.

[19] T.D. Tawari, F.A. Zenz, Evaluating cyclone efficiencies from stream compositions, Chem. Eng. 91 (9) (1984) 69–73.

[20] C.R. Ghadiri, A.C. Hoffman, A critique of two models for cyclone performance, AIChE J. 37 (1991) 285–289.